Pravara Med Rev; September 2026, 18 (03), 108-117
DOI: 10.36848/PMR/2026/8500000328

Original article

Field-Based 3D-QSAR Modelling and Molecular Docking Analysis of Keap1 Inhibitors

Naveen Pathakala[1*], Sindhu Gugulothu[2], Mohammed Amer Rohaid[3]

[1] School of Pharmacy, Anurag University, Hyderabad, Telangana, India 500088.
[2, 3] Department of Pathology, New Anglia University, Anguilla, George Hill (AI-2640), British Overseas Territory
Corresponding author - Dr P. Naveen

Abstract

This study investigated the structural and physicochemical determinants governing the inhibition of Kelch-like ECH-associated protein 1 (Keap1) by integrating field-based 3D-QSAR modelling, molecular docking, and molecular dynamics (MD) simulations. Inhibition of Keap1 disrupts the Keap1–Nrf2 interaction, thereby preventing the proteasomal degradation of nuclear factor erythroid 2-related factor 2 (Nrf2), promoting its activation, and enhancing cellular antioxidant defence against oxidative stress. A robust field-based 3D-QSAR model was developed using a diverse set of Keap1 inhibitors, demonstrating excellent predictive performance with statistical parameters of r^2 = 0.876, q^2 = 0.846, $RMSE_{CV}$ = 0.242, and RMSE Test = 0.254. Molecular docking against the selected crystal structure (PDB ID: 9F2Q) produced binding energies of −12.33, −10.80, and −8.20 kcal/mol for the co-crystallized ligand, CHEMBL319587, and CHEMBL527178, respectively, indicating favourable binding within the Keap1 active site. MD simulation analyses, including root mean square deviation (RMSD), root mean square fluctuation (RMSF), and protein–ligand interaction profiling, demonstrated the structural stability and constant binding of CHEMBL319587 throughout the simulation. These findings provide valuable insights into the molecular features governing Keap1 inhibition and offer a rational framework for the design and optimization of potent Keap1 inhibitors with enhanced therapeutic potential.

Key words: *Keap1, Nrf2, 3D-QSAR, MD Simulation, Neuroprotection*

1. Introduction

Numerous chronic illnesses, such as metabolic disorders, neurological disorders, cancer, andinflammatory disea ses, have oxidative stress as a major contributing factor. The nuclear factor erythroid 2-related factor 2 (Nrf2) pathway regulates antioxidant and cytoprotective genes as a key sensor in cellular defence mechanisms against oxidative damage. Under physiological conditions, Nrf2 is repressed by cytosolic Kelch-like ECH-associated protein 1 (Keap1), which promotes its ubiquitination and proteasomal degradation. Inhibition of Keap1 detaches this interaction, resulting in stabilization and nuclear translocation of Nrf2 and augmentation of cellular antioxidant responses. (Crisman, E., Duarte, P., 2023). The Keap1-Nrf2 signalling pathway is a critical regulator of the cellular defence response to endogenous and external stress induced by reactive oxygen species (ROS) (Kansanen, E., 2012). Due to the important role of Keap1 in the regulation of oxidative stress, Keap1 has been developed as a potential therapeutic target for the treatment of free radical-mediated illnesses (Figure 1). The Kelch domain of Keap1 binds to several identified small-molecule Keap1 inhibitors and inhibits its interaction with Nrf2. Despite these developments, a complete understanding of the structural characteristics that drive Keap1 inhibition is still required for the rational design and optimization of effective inhibitors. Reduced Nrf2 signalling is a key contributor to the pathogenesis of neurodegenerative disorders, by exacerbating oxidative stress and mitochondrial dysfunction, ultimately leading to progressive neuronal damage. Activation of Nrf2 protects neurons by inhibiting neuroinflammation, maintaining mitochondrial function and improving cell survival (Cuadrado A, Rojo AI, et al 2019). The Keap1-Nrf2 pathway also contributes to cardiovascular disorders such as atherosclerosis, hypertension, cardiac ischemia-reperfusion injury and heart failure. Emerging evidence suggests that activation of Nrf2 protects vascular function by mitigating endothelial dysfunction, reducing lipid peroxidation, and attenuating inflammatory cytokine production, thereby promoting vascular homeostasis (Saha et al., 2020).

PMR P ISSN: 0975-0533, E ISSN: 0976-0164

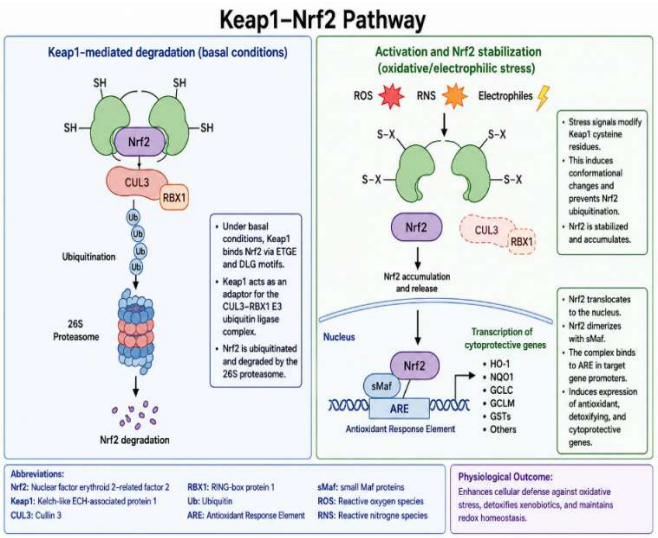


Figure 1: Molecular Mechanism of Keap1-Mediated Regulation of Nrf2 Signalling Pathway.

2. Methodology

2.1 Molecular Dataset Curation and Preparation

A list of Kelch-like ECH-associated protein 1 (Keap1) inhibitors was collected from the pChEMBL database. Duplicate entries, salts, and compounds with ambiguous or inconsistent biological activity data were eliminated. Only compounds with experimentally determined activities from comparable biochemical assays were retained to ensure dataset reliability. Compounds with pChEMBL values ≥ 5 were selected, yielding a final dataset of 226 potent Keap1 inhibitors. The two-dimensional (2D) structures were prepared and saved in SDF format, then energy-minimised using Cresset Flare (Cresset, UK) to generate stable, low-energy conformations. Biological activity values were converted to pActivity values (−log scale) where applicable. Molecular protonation states were determined at physiological pH (7.0) before QSAR model development (Zdrazil B. et al 2024).

2.2 Conformational analysis and molecular alignment

The crystal structure of Keap1 (PDB ID: 9F2Q) was obtained from the RCSB Protein Data Bank (PDB) (Pathakala N et al., 2022). The co-crystallised ligand was extracted and used as the reference for molecular alignment. Binding-site information derived from this ligand guided ligand superposition. The curated dataset was randomly divided into stratified training and test subsets to ensure that the distribution of biological activity was similar between the subsets. A conformational search was performed for all ligands in Flare to generate energetically favourable conformations. Up to 100 conformers per molecule were generated using a gradient cutoff of 0.10 kcal/mol. Redundant conformers were removed using an RMSD threshold of 0.50 Å and an energy window of 3.00 kcal/mol. Molecular alignment was performed using a reference ligand-based approach that incorporated field similarity and common substructural features. The resulting alignments were visually inspected to confirm accurate overlap with the reference ligand and consistency across the dataset (Narayanan D, et al.2024).

2.3 Field-based 3D-QSAR model development

Field-based three-dimensional quantitative structure activity relationship (3D-QSAR) models were developed using the Forge module of Cresset Flare. Partial Least Squares (PLS) regression utilising the SIMPLS algorithm was employed for the correlation of molecular field descriptors with biological activity. Electrostatic and steric (shape) descriptors were calculated using the extended electron distribution (XED) force field. The aligned compounds were used to construct the QSAR models, and the set was divided randomly into a training set (70%) and a test set (30%) for model building and external validation, respectively. Up to 20 PLS components were evaluated in model optimisation. The minimum spacing between the sample points was kept at 1.0 Å. The predictive performance and robustness of the models were evaluated on the basis of statistical parameters including coefficient of determination (R^2), leave-one-out cross-validated coefficient (q^2), root mean square error (RMSE) and predictive RMSE. The final model was chosen based on good statistical reliability, high predictive ability and low chance correlation risk according to the criteria proposed by Golbraikh and Tropsha (2002) & Sowmya Andole et al. (2023).

2.4 Molecular Docking Studies

Based on the field-based 3D-QSAR results, four representative ligands, comprising two highly active and two low-activity compounds, were selected for molecular docking to enable comparative analysis of binding interactions (Sahoo NK et al .2025, Pathakala N et al., 2021). The ligands were prepared in Cresset Flare by assigning protonation states at physiological pH (7.0), followed by energy minimisation using molecular mechanics. Where applicable, the conformations obtained from the QSAR alignment were retained to maintain consistency between the ligand-based and structure-based studies (Friesner et al., 2004; Cresset, 2024; Ahmad AVD et., al 2025).

2.5 Molecular Dynamics Simulations

Molecular dynamics (MD) simulations of selected Keap1 protein–ligand complexes (PDB ID: 9F2Q) were carried out in Desmond (Schrödinger). The systems were prepared using the OPLS force field in an orthorhombic TIP3P water box and neutralized with Na^+/Cl^- ions at physiological salt concentration (~0.15 M). Simulations were performed in the NPT ensemble for 100 ns (one replicate for 10 ns) at 300 K. We assessed trajectories by calculating the root mean square deviation (RMSD) of protein and ligand, the root mean square fluctuation (RMSF) of protein and ligand, the stability of secondary structure, and the persistence of protein–ligand interactions (Roos K, Wu C, Damm W, et al., 2019).

3 Results

A field-based three-dimensional quantitative structure–activity relationship (3D-QSAR) model was constructed in Cresset Flare using a curated set of Keap1 inhibitors. The model was developed based on ligand-derived aligned conformations to ensure that the molecular alignment was consistent with the experimentally established binding orientation within the Keap1 binding site. Figure 2 illustrates the protein field points and their interactions with the co-crystallised ligand. Following conformational analysis of the dataset compounds, the training-set molecules were aligned to generate their corresponding field-point patterns. Superimposition of the aligned compounds with the co-crystallised ligand revealed common field-point features associated with ligand–protein interactions. Figure 3 presents the 3D molecular representations of the aligned training-set compounds with their corresponding field points. Positive electrostatic, negative electrostatic, hydrophobic, and van der Waals fields are represented in red, cyan, gold, and yellow, respectively. Highly active compounds (H1 and H2) and low-active compounds (L1 and L2) are highlighted for comparison.

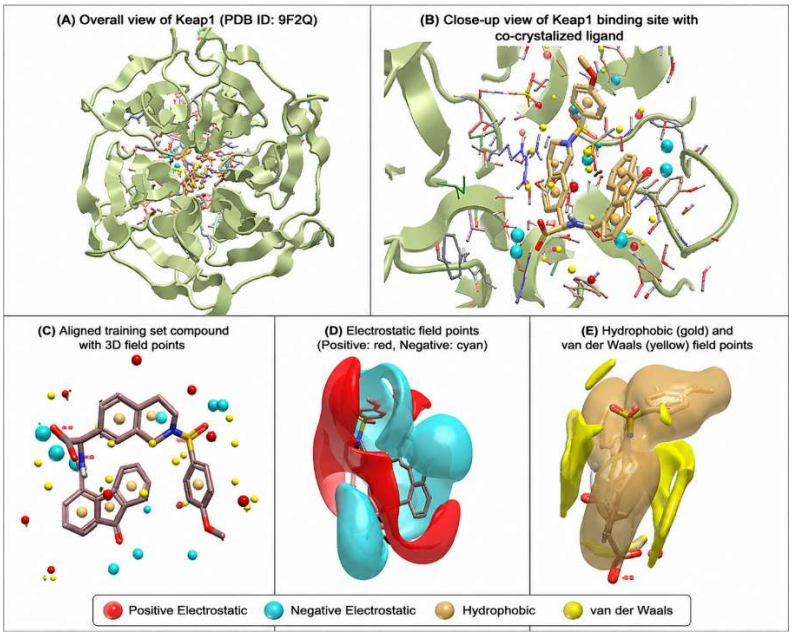


Figure 2 illustrates the aligned training-set compounds and their corresponding three-dimensional field points for PDB ID 9F2Q, where red, cyan, gold, and yellow represent positive electrostatic, negative electrostatic, hydrophobic, and van der Waals field points, respectively.

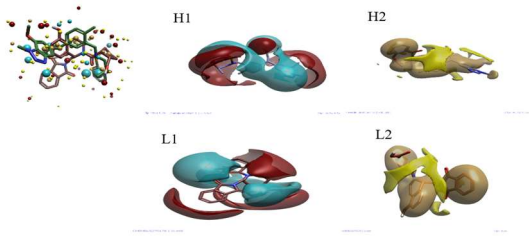


Figure 3: 3D alignment of the training set compounds and their corresponding molecular field points. Positive electrostatic, negative electrostatic, hydrophobic, and van der Waals field points are represented in red, cyan, gold, and yellow, respectively. H1 and H2 denote highly active training set compounds, whereas L1 and L2 represent low-activity compounds.

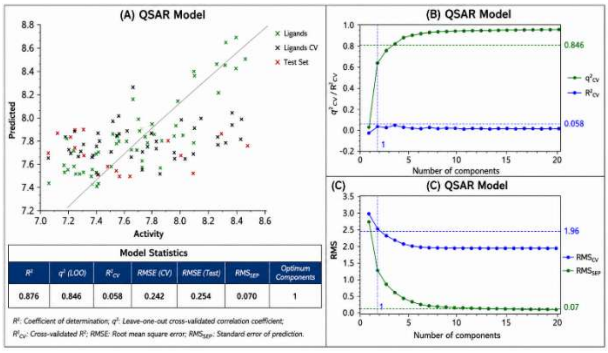


Figure 4 (A) Predicted activity against activity. (B) Regression analysis of the QSAR model. (C) Plot of RMSE

Table 1: Statistical Results for field-based 3D QSAR prediction

Model	r^2 Training set	q^2 Training set	RMSE cv	RMSE $_{Test}$
3D Field	0.876	0.846	0.242	0.254

Coefficient of determination R^2, Cross-validation correlation q2, Root Mean Square Error = RMSE

A field-based 3D-QSAR model was developed using Cresset Flare v9.0. The model identified regions around the aligned molecules where variations in molecular fields were associated with changes in biological activity. The statistical performance parameters of the model are summarised in Table 1 and in Figure 4. The model showed excellent performance, with high training ($r^2 = 0.876$) and cross-validated ($q^2 = 0.846$) correlation coefficients, indicating a good fit and strong internal predictivity. Electrostatic coefficient map of the field model showing regions favourable for elevated biological activity. The positive electrostatic potential regions are shown as blue cubes, indicating that positively charged groups or hydrogen bond donor groups contribute to activity, while the negative electrostatic potential regions are shown as red cubes, indicating that negatively charged groups or hydrogen bond acceptor groups are responsible for activity. Steric coefficient map showing regions contributing to biological activity. Green cubes represent favourable steric regions, where the presence of larger substituents is expected to increase activity by increasing hydrophobic interactions or by better filling the binding site. On the other hand, purple/magenta cubes indicate the areas where small substituents are preferred. A larger substituent at these positions may lead to steric hindrance and a reduction in ligand–protein interactions (Figure 5).

Table 2: Molecular docking results

Parameter	Co-crystal ligand	Highest Activity ligand	Lowest Activity ligand
LF_{DG} Dock score	-12.33 kcal/mole	-10.8 kcal/mole	-8.2 kcal/mole

Molecular docking was performed to evaluate the binding interactions between the ligands and the Kelch-like ECH-associated protein 1 (Keap1) Kelch domain using the crystal structure PDB ID: 9F2Q. The co-crystallised ligand, (R)-2-(2-((4-methoxyphenyl) sulfonyl)-1,2,3,4-tetrahydroisoquinolin-7-yl)-2-(9-oxo-9H-fluorene-4-

carboxamido) acetate (THIQ–Fluorenone Sulfonamide), was first extracted and subsequently redocked into the Keap1 binding site to validate the docking results.

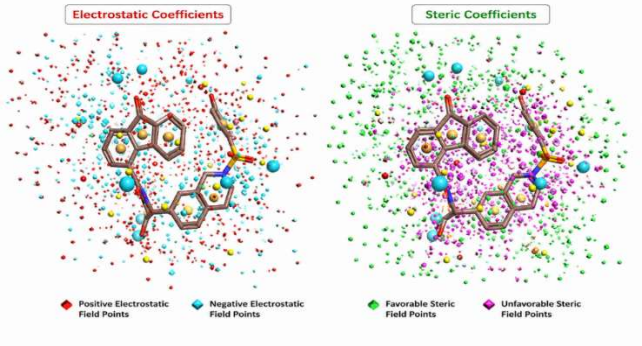


Figure 5: Electrostatic and steric coefficient maps of the field model for the most potent compound, showing positive and negative electrostatic and steric field points that highlight regions with a significant contribution to higher biological activity

The co-crystallized ligand THIQ–Fluorenone Sulfonamide exhibited a docking score of −12.33 kcal/mol, indicating strong binding affinity toward Keap1. Direct hydrogen bonds were formed with Arg415 (salt bridge, P1), Gln530 (P5), Tyr572 (P4), and Ser555 (P5), while water-mediated interactions involving HOH1043, HOH1046, and HOH1048 further stabilized the complex through contacts with Tyr525, Ser525/Gln530, and Asn414, respectively. The ligand was additionally stabilized by π–π interactions with Tyr334, Tyr572, and Phe577, cation–π interactions with Arg483 and Arg415, and hydrophobic contacts with Val478, Ile461, and Leu557 (Figure 6). CHEMBL319587 exhibited a docking score of −10.8 kcal/mol, indicating favourable binding to the Keap1 Kelch domain. The ligand formed direct hydrogen bonds with Arg415 (salt bridge, P1), Tyr572 (P4), Ser555 (P5), Ser508 (P5), and the backbone of Gly509 (P2). Water-mediated interactions via HOH A901, HOH A117, and HOH A104 further stabilized the complex through Ser555, Arg415, and Ile416, respectively. Additional stabilisation was provided by π–π interactions with Tyr572, a cation–π interaction with Arg415, and hydrophobic contacts involving Ile416, Leu557, Leu365, and Val residues (Figure 7). CHEMBL527178 exhibited a docking score of −8.2 kcal/mol, indicating moderate binding affinity toward the Keap1 Kelch domain. The ligand formed direct hydrogen bonds with Arg415 (salt bridge, P1), Arg483 (P2), Ser555 (P5), Tyr525 (P4), and Ser508 (P5). Water-mediated interactions via HOH A1046, HOH A1079, HOH A1071, and HOH A996 further stabilized the complex through Ser555, Gln, Tyr525, and Arg483, respectively. Additional stabilization was provided by π–π interactions with Tyr525, cation–π interactions involving Arg415 and Arg483, and hydrophobic contacts with nearby Leu residues within the binding pocket. Comparative docking analysis demonstrated that the co-crystallized ligand THIQ–Fluorenone Sulfonamide exhibited the strongest binding affinity toward the Keap1 Kelch domain, with a docking score of −12.33 kcal/mol, followed by CHEMBL319587 (−10.8 kcal/mol) and CHEMBL527178 (−8.2 kcal/mol). The co-crystallized ligand established the most extensive interaction network, including multiple direct and water-mediated hydrogen bonds, π–π stacking, cation–π interactions, and hydrophobic contacts, resulting in a highly stable protein–ligand complex. CHEMBL319587 displayed a similar binding mode but formed fewer stabilizing interactions, whereas CHEMBL527178 showed the least favourable binding, with a reduced interaction network despite retaining key hydrogen bonds and hydrophobic contacts.

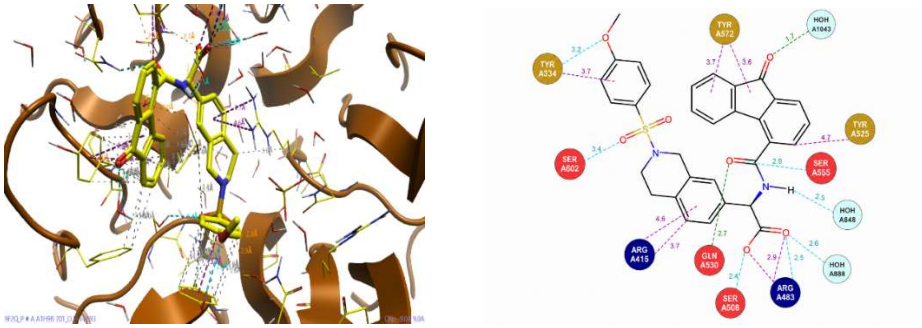


Figure 6: 3D, 2D molecular docking images of cocrystal ligand THIQ–Fluorenone Sulfonamide with PDB ID 9F2Q

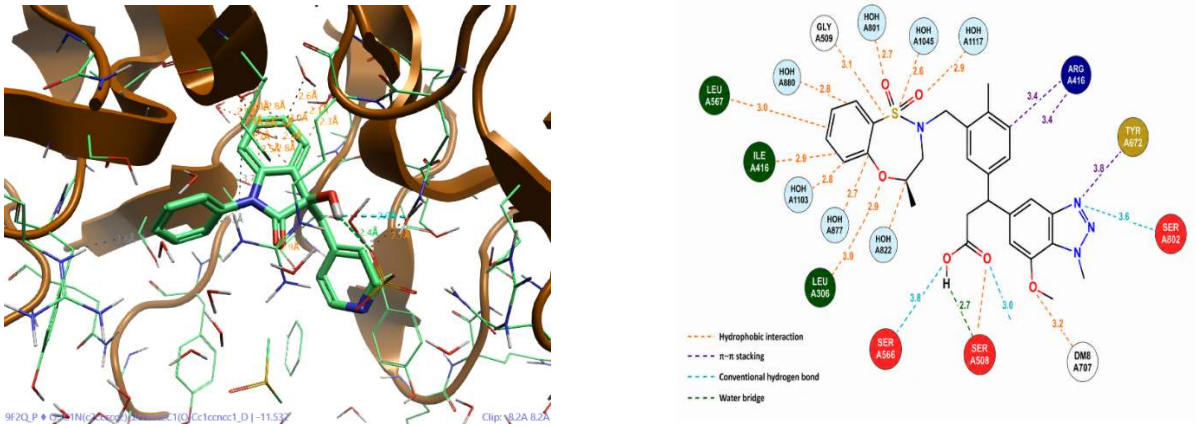


Figure 7: 3D, 2D molecular docking images of Highest activity ligand CHEMBL319587 with PDB ID 9F2Q

Molecular Dynamics Simulations

To verify the docking results, the co-crystallised ligand (THIQ–Fluorenone Sulfonamide) and the highest (CHEMBL319587) and lowest-active (CHEMBL527178) compounds were subjected to 100 ns molecular dynamics simulations in the TIP3P water model using the Desmond module of the Schrödinger Suite with the OPLS force field. The Keap1 protein (PDB ID: 9F2Q) exhibited a stable RMSD of approximately 0.8–1.0 Å during the first 15 ns, followed by a slight increase to 1.2–1.3 Å around 15 ns, which remained consistent throughout the simulation. An average protein RMSD of less than 1.5 Å demonstrates high structural stability of the protein throughout the 100 ns molecular dynamics simulation. The co-crystallised ligand THIQ- Fluorenone Sulfonamide showed a stable RMSD of 1.3-2.2 Å, which indicated strong retention within the P1-P5 sub-pockets, which is consistent with its docking score of -12.33 kcal/mol. CHEMBL319587 showed low RMSD values (2-5 Å) till 40 ns, with a docking score-10.8 kcal/mole indicating stable binding followed by increased fluctuations that may indicate partial displacement from the binding pocket. The lowest activity compound CHEMBL527178 RMSD fluctuates from 3-11Å between 2 and 10ns, and several fluctuations indicate low binding stability. RMSF values of 0.6–2.1 Å, 2.7–2.9 Å, and 6.0–10.0 Å, respectively, indicate progressively greater residue flexibility of the co-crystallised ligand and the highest activity ligand CHEMBL319587, and the lowest activity ligand CHEMBL527178 (Figure 8).

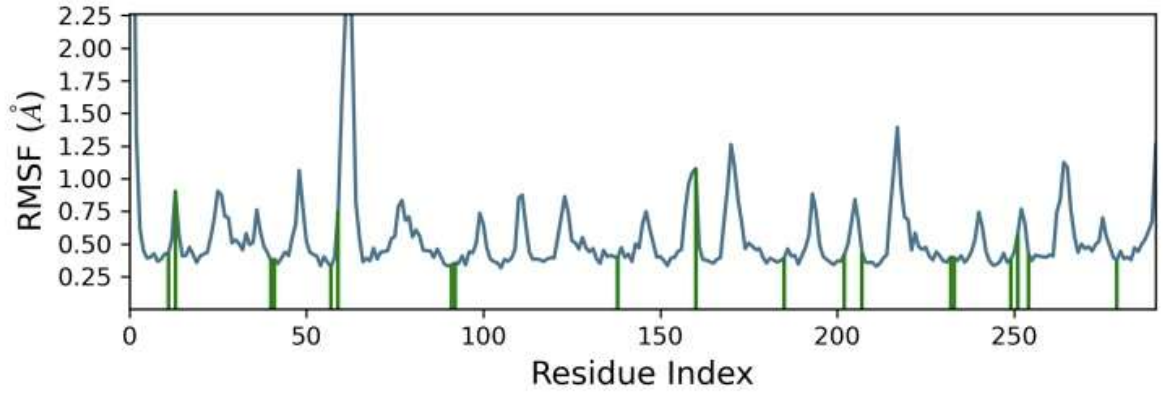


Figure 8: MD Simulation Protein-ligand complex of Kap1 (PDB ID: 9F2Q) for 100 ns

Analysis of the C-alpha RMSF profile indicates that the protein maintained overall structural stability throughout the simulation, with the majority of residues exhibiting fluctuations of less than 0.6 Å. Localised increases in flexibility are evident at the N-terminus and in several loop regions near residues ~60, ~170, ~220, and ~270, where the RMSF reaches approximately 1.2–2.3 Å. The interaction analysis revealed distinct binding patterns among the three ligand–protein complexes. The first ligand established the most favourable interaction network, comprising multiple hydrophobic contacts with Tyr525, Tyr572, Tyr334, and Ala556, together with polar interactions involving Ser555 and Ser602. Additionally, π–π stacking interactions with Tyr525 and Tyr572 further stabilized the aromatic scaffold of the ligand, while limited solvent exposure indicated efficient accommodation within the binding pocket. In contrast, the highest activity ligand exhibited no significant protein-mediated

interactions and remained largely solvent-exposed, suggesting weak binding and poor stabilization within the active site. The lowest activity ligand displayed an intermediate interaction profile, forming a single polar interaction with Ser340 of relatively low occupancy (~39%) while remaining partially solvent-exposed. Overall, the first ligand demonstrated the strongest interaction network and is therefore expected to possess the highest binding stability and affinity among the three complexes.

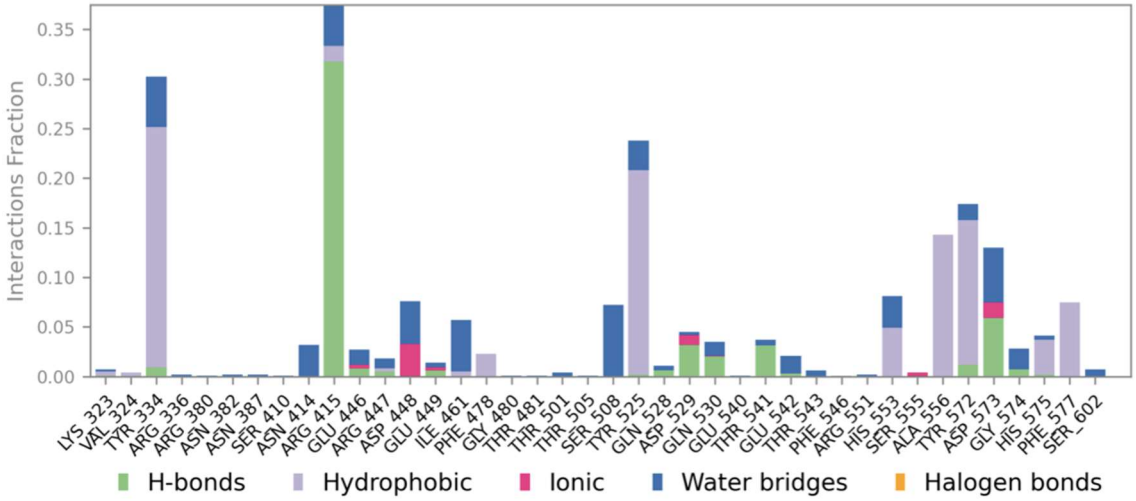


Figure 9: MD Simulation; Highest-activity compound CHEMBL319587 interaction with 9F2Q

Protein–ligand interaction analysis showed that the co-crystallised ligand maintained stable hydrogen bonds with Ser555 and Ser602, along with hydrophobic interactions involving Tyr334, Tyr525, Tyr572, and Ala556 and several water-mediated contacts. CHEMBL319587 formed persistent hydrogen bonds with Glu445, Asp573, and Glu541, supported by hydrophobic and water-mediated interactions (Figure 9). The ligand remained relatively stable during the 100 ns simulation, with temporary RMSD changes accompanied by variations in SASA, PSA, MolSA, and rGyr (Figure 10). No intramolecular hydrogen bonds were observed.

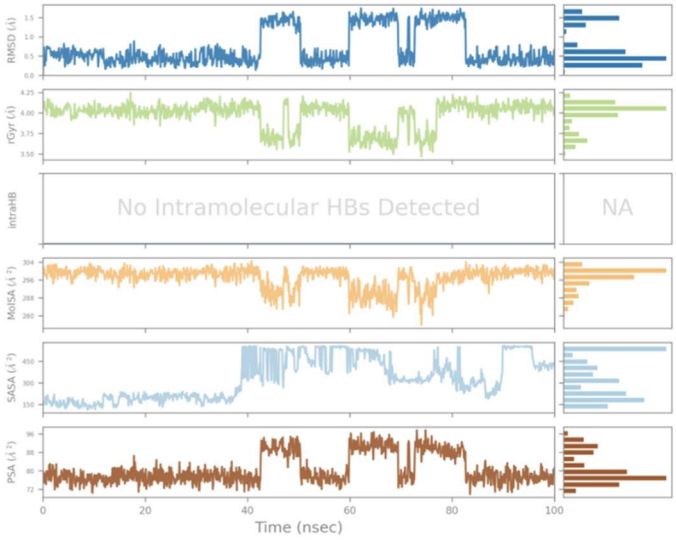


Figure 10: MD simulation: ligand RMSD, radius of gyration (rGy), intramolecular hydrogen bonds (intraHB), molecular surface area (MolSA), solvent accessible surface area (SASA) and polar surface area (PSA) plot.

Discussion

An integrated computational methodology was employed to identify potential Keap1 inhibitors involving data curation, virtual screening, molecular docking, 3D-QSAR and molecular dynamics (MD) simulations. Docking and 3D-QSAR studies identified critical binding interactions and structural characteristics influencing activity, and MD simulations assessed the stability of the complexes. This integrated strategy allows us to prioritise prospective Keap1 inhibitors for future experimental validation (Lanka G et al, 2023). Observed overlap of field-

point features indicates that the aligned training compounds share key steric and electrostatic characteristics with the co-crystallised ligand. These conserved interaction features may contribute to Keap1 binding and biological activity, providing a structural basis for the subsequent 3D-QSAR analysis in Figure 2. The field-point distribution revealed differences in the steric, electrostatic, and hydrophobic features of highly and poorly active compounds. These variations may contribute to differences in Keap1 inhibitory activity and provide useful structural insights for interpreting the 3D-QSAR model in Figure 3. The field-point maps provide insights into the structural features influencing Keap1 inhibitory activity. Prominent red and cyan electrostatic field points indicate regions where favourable electrostatic interactions may contribute to stronger activity, offering useful guidance for understanding the observed structure–activity relationships. The electrostatic map suggests that positively charged or hydrogen-bond-donating groups may be favourable in blue regions, whereas negatively charged or hydrogen-bond-accepting groups may enhance activity in red regions. The steric map indicates that larger substituents may be tolerated or preferred in green regions, potentially improving binding through better pocket occupancy, while smaller substituents are favoured in purple/magenta regions to minimise steric interference. These field-based features provide useful structural guidance for optimising Keap1 inhibitors. The molecular docking data obtained for the highly active ligand CHEMBL319587 with the target protein PDB ID 9F2Q are shown in Table 2, which indicates a good binding affinity of −10.8 kcal/mol. The affinity was slightly lower than that of the co-crystallised ligand (−12.33 kcal/mol), yet this finding suggests a strong positive interaction between CHEMBL319587 and the target protein. A stable RMSD was observed at 1.3-2.2 Å and 2- 5 Å with 9F2Q for the co-crystallised ligand and the highest activity ligand CHEMBL319587, respectively. The persistent interactions of the co-crystallised ligand indicate strong binding-site stabilisation. CHEMBL319587 maintained key polar interactions, particularly with Glu445, supporting its stable binding conformation. The observed changes in RMSD and solvent-accessibility parameters likely represent transient conformational adjustments rather than ligand dissociation (Grewal S, et al, 2025). RMSF values of 0.6–2.1 Å, 2.7–2.9 Å, and 6.0–10.0 Å, respectively, indicating progressively greater residue flexibility of the co-crystallised ligand and the highest activity ligand CHEMBL319587, and the lowest activity ligand CHEMBL527178. RMSF measures the average positional fluctuation of each atom or residue around its mean position during a molecular dynamics (MD) simulation. It is commonly used to evaluate the flexibility of different regions of a protein. RMSF measures the average fluctuation of atoms or residues around their mean positions during the simulation. Lower RMSF values indicate a rigid and stable binding pocket, whereas higher values reflect greater local flexibility. The protein exhibited RMSF values ranging from 0.3 to 0.7 Å throughout the simulation. In comparison, the protein complexes with the crystallised ligand, the highest-activity compound, and the lowest-activity compound showed RMSF values of 0.6–2.1 Å, 2.7–2.9 Å, and 6.0–10.0 Å, respectively, indicating progressively greater residue flexibility (Vander Meersche Y. al 2024). The integrated 3D-QSAR, molecular docking and molecular dynamics studies collectively provided a consistent picture for the favourable binding nature of CHEMBL319587 toward Keap1. The field-derived QSAR results indicated important steric and electrostatic features related to activity, and docking confirmed its good interaction in the 9F2Q binding pocket. The MD results also revealed that CHEMBL319587 retained essential interactions with Glu445 and had reasonable conformational stability in the course of the simulation. Taken together, these findings identify CHEMBL319587 as a promising Keap1 inhibitor and provide useful structural information for the rational optimization and future experimental validation of novel Keap1 modulators.

Conclusion

A field-based 3D-QSAR model was developed using 226 Keap1 modulators and showed good predictive performance. The model highlighted important electrostatic and steric features associated with inhibitory activity. Molecular docking followed by 100 ns molecular dynamics simulations further supported the favourable binding and stability of the selected active compounds within the Keap1 binding pocket. Overall, these findings provide useful mechanistic insights into the activity of CHEMBL319587 and offer an integrated computational approach for guiding the rational design of new Keap1 inhibitors for the treatment of oxidative stress-related disorders.

Acknowledgments

The authors sincerely acknowledge the financial support received from the Research and Development (R&D) Cell, Anurag University, Hyderabad, through the Seed Money Research Grant (Grant No. **AU/R&D/Seed Money/September-2024/59**). The authors are also grateful to the School of Pharmacy, Anurag University,

Hyderabad, for the procurement of Cresset Software and for providing the research infrastructure and facilities that enabled the successful completion of this work.

Reference

1. Crisman E, Duarte P, Daudén E, Cuadrado A, Rodríguez-Franco MI, López MG, et al. KEAP1-NRF2 protein-protein interaction inhibitors: design, pharmacological properties and therapeutic potential. Med Res Rev. 2023;43(1):237-287.
2. Kansanen E, Jyrkkänen HK, Levonen AL. Activation of stress signaling pathways by electrophilic oxidized and nitrated lipids. Free Radic Biol Med. 2012;52(6):973-982.
3. Cuadrado A, Rojo AI, Wells G, Hayes JD, Cousin SP, Rumsey WL, et al. Therapeutic targeting of the NRF2 and KEAP1 partnership in chronic diseases. Nat Rev Drug Discov. 2019;18(4):295-317.
4. Saha S, Buttari B, Panieri E, Profumo E, Saso L. An overview of Nrf2 signaling pathway and its role in inflammation. Molecules. 2020;25(22):5474. doi:10.3390/molecules25225474.
5. Rojo de la Vega M, Chapman E, Zhang DD. NRF2 and the hallmarks of cancer. Cancer Cell. 2018;34(1):21-43. doi:10.1016/j.ccell.2018.03.022.
6. Bellezza I, Giambanco I, Minelli A, Donato R. Nrf2-Keap1 signaling in oxidative and reductive stress. Biochim Biophys Acta Mol Cell Res. 2018;1865(5):721-733. doi:10.1016/j.bbamcr.2018.02.010.
7. Singh E, Matada GSP, Dhiwar PS, Patil RB, Pal R. In-silico based discovery of potential Keap1 inhibitors using the strategies of pharmacophore screening, molecular docking, and MD simulation studies. Bioimpacts. 2025;15:30335. doi:10.34172/bi.30335.
8. Zdrazil B, Felix E, Hunter F, Manners EJ, Blackshaw J, Corbett S, et al. The ChEMBL database in 2023: a drug discovery platform spanning multiple bioactivity data types and time periods. Nucleic Acids Res. 2024;52(D1):D1180-D1192. doi:10.1093/nar/gkad1004.
9. Pathakala N, Patangay S, Bantal V. Nevirapine backwards brain excitotoxicity in cerebral ischemic stroke, to screen the activity using molecular docking studies and middle cerebral artery occlusion model in Wistar rats. NeuroQuantology. 2022;20(6):2498-2514.
10. Narayanan D, Bach A, Gajhede M. Crystal structure of Keap1 kelch domain in complex with a tetrahydroisoquinoline-based small molecule inhibitor at 1.2 Å resolution [Internet]. RCSB Protein Data Bank; 2024 [cited 2026 Oct 7]. PDB ID: 9F2Q. Available from: https://doi.org/10.2210/pdb9f2q/pdb
11. Golbraikh A, Tropsha A. Beware of q²! J Mol Graph Model. 2002;20(4):269-276. doi:10.1016/S1093-3263(01)00123-1.
12. Andole S, Thumma G, Alavala RR, Gangarapu K. Field-based 3D-QSAR for tyrosine protein kinase JAK-2 inhibitors. J Biomol Struct Dyn. 2024;42(10):5321-5333. doi:10.1080/07391102.2023.2226723.
13. Sahoo NK, Gollamudi R, Reddy BM, Pathakala N, Rath D, Panigrahy UP, et al. Comprehensive computational investigation of Rynchotechum ellipticum for neuro-pharmacological activity: molecular docking, molecular dynamics and pre-ADMET analysis. Adv J Chem A. 2025;8(12):2059-2075.
14. Pathakala N, Patangay S, Bantal V. Neuroprotective potential of efavirenz nanoparticles on cerebral ischemic stroke by middle cerebral artery occlusion in Wistar rats. Int J Pharm Res. 2021;13(2):1971-1980. doi:10.31838/ijpr/2021.13.02.248.
15. Ahmad AVD, Shaikh MS, Yasar Q, Khan MM, Pathakala N, Mamidisetti YD, et al. Unexplored enigma in Flemingins against cholangiocarcinoma: a network pharmacology and molecular docking approach to predict molecular mechanisms. Chem Methodol. 2025;9(7):610-630.
16. Friesner RA, Banks JL, Murphy RB, Halgren TA, Klicic JJ, Mainz DT, et al. Glide: a new approach for rapid, accurate docking and scoring. 1. Method and assessment of docking accuracy. J Med Chem. 2004;47(7):1739-1749. doi:10.1021/jm0306430.
17. Roos K, Wu C, Damm W, Reboul M, Stevenson JM, Lu C, et al. OPLS3e: extending force field coverage for drug-like small molecules. J Chem Theory Comput. 2019;15(3):1863-1874.
18. Lanka G, Begum D, Banerjee S, Adhikari N, Yogeeswari P, Ghosh B. Pharmacophore-based virtual screening, 3D QSAR, docking, ADMET, and MD simulation studies: an in-silico perspective for the identification of new potential HDAC3 inhibitors. Comput Biol Med. 2023;166:107481. doi:10.1016/j.compbiomed.2023.107481.

19. Grewal S, Deswal G, Grewal AS, Guarve K. Molecular dynamics simulations: insights into protein and protein ligand interactions. Adv Pharmacol. 2025;103:139-162. doi:10.1016/bs.apha.2025.01.007.
20. Vander Meersche Y, Cretin G, Gheeraert A, Gelly JC, Galochkina T. ATLAS: protein flexibility description from atomistic molecular dynamics simulations. Nucleic Acids Res. 2024;52(D1):D384-D392. doi:10.1093/nar/gkad1084.